Strategy Sets the Scene: Genetic architecture of linalool resistance in *Botrytis cinerea*

Melanie Madrigal*[1], Jenna C. Moseley[1], Daniel J. Kliebenstein[2], Jordan A. Dowell[1,3]

Department of Biological Sciences, Louisiana State University, Baton Rouge, Louisiana 70803, USA[1]

Department of Plant Sciences, University of California, Davis, California 95616, USA[2]

Department of Plant Pathology and Crop Physiology, Louisiana State University AgCenter, Baton Rouge, Louisiana 70803, USA[3]

*Correspondence to: madrigal.melanie007@gmail.com

Emails of authors: moseleyjc05@gmail.com; kliebenstein@ucdavis.edu; jordan.dowell@gmail.com

Abstract:

Botrytis cinerea is a necrotrophic fungal pathogen that infects thousands of plant species. During infection, these diverse plant hosts produce different specialized metabolites that can inhibit pathogen growth and shape pathogen fitness. However, the genetic architecture of pathogen resistance toward individual host defense metabolites remains poorly understood. To address this question, we exposed 83 *B. cinerea* isolates to the metabolite linalool and quantified metabolic and structural responses. Exposure revealed extensive phenotypic diversity across isolates. Genome-wide association identified 101 genes of interest associated with membrane transport and stress response regulation. Genetic associations were stronger for morphological traits than for metabolic traits, suggesting that hyphal architecture may have a complex genetic architecture contributing to linalool resistance. Together, these results establish natural variation in linalool

response and provide candidate loci for understanding how generalist pathogens respond to host-derived chemical defenses.

Article Summary:

To understand how a generalist pathogen responds to host defenses, we asked how *Botrytis cinerea* responds to linalool, a widespread monoterpene involved in plant defense. We exposed 83 *B. cinerea* isolates to 1000 µM of linalool for 72 hours and quantified metabolic traits (growth curves and growth dynamics over time) and morphological traits (hyphal network features). Using GWA, we linked phenotypic variation to genetic variants. Results indicate substantial natural variation in linalool resistance and distinct genetic architectures across trait classes: metabolic responses are driven by a relatively small number of loci with larger effects, whereas structural/morphological responses appear more polygenic.

Introduction

Plant-pathogen interactions are dynamic, often shaped by host and pathogen genetic factors, as well as by other complex evolutionary and ecological processes. Plants respond to pathogens through multiple defenses, including changes in metabolism, such as the induction of the jasmonic or salicylic acid pathways. These signaling pathways coordinate the production of specialized metabolites (SMs). These SMs vary in structure, abundance, and toxicity across different plant species, serving as chemical barriers that can inhibit pathogen growth[24]. Among SMs, volatile organic compounds (VOCs) can mediate information transfer between hosts and their pathogens, along with directly inhibiting pathogen growth[29]. VOCs are released in response to herbivore or pathogen attack and abiotic stressors, indicating damaged plant tissue or compromised immunity. At the same time, these VOCs can prime plants for future attacks, such that post-exposure plants mount more severe responses when they are attacked [10,15,32]. Thus, VOCs have been a major target for plant-derived pesticides due to their low molecular weight, high vapor pressure, low water solubility, and their ability to mediate resistance to multiple

53 biological targets.[59] Due to the multifaceted effects of VOCs on pathogens and reduced
54 environmental persistence, they are an attractive alternative to conventional synthetic
55 pesticides.[59]

56 As VOC profiles vary with host identity[62] and environment,[25] they provide rich
57 information about host identity and condition[16]. Microorganisms may perceive these VOCs as a
58 signal of host vulnerability. For example, the slime mold *Physarum polycephalum* exhibits
59 chemotaxis toward/away from multiple VOCs [35], with linalool causing *P. polycephalum* to direct
60 its growth away from the compound. Among plant-associated habitats, such as the rhizosphere,
61 fungi respond to plant VOCs, which can modulate fungal development and influence regulatory
62 pathways associated with stress responses and metabolism [27].

63 The generalist necrotrophic pathogen *Botrytis cinerea* provides an ideal system for
64 investigating fungal responses to VOCs. *B. cinerea* infects thousands of hosts with few genetic
65 indicators of host specificity[44] despite evidence that gene expression responses can be host
66 specific[49]. As such, virulence in *B. cinerea* is polygenic, with small-effect loci contributing to
67 infection success rather than a few major-effect loci [7,14,55]. Moreover, it relies on a multitude of
68 broad-spectrum virulence strategies, with genome-wide association studies demonstrating that
69 variation in virulence genes is distributed across the genome and shows little enrichment for
70 specific pathways or compartments [14,55]. As a necrotrophic pathogen, *B. cinerea* relies not only
71 on host tissue degradation but also on its capacity to overcome host defenses through a variety of
72 mechanisms, including enzymatic detoxification and transporter-mediated efflux [63,66]. Further,
73 the sheer diversity of hosts suggests that *B. cinerea* individuals may be exposed to a wide range
74 of lineage-specific and general VOCs, necessitating strategies to deal with an array of complex
75 SMs and VOCs alike.

76 Among plant VOCs, linalool is found in over 200 monocotyledonous and dicotyledonous
77 plant species, belonging to over 50% of plant families [4]. Linalool is an acyclic monoterpene
78 alcohol that is produced through the methylerythritol phosphate (MEP) pathway, where geranyl
79 diphosphate (GPP) serves as its immediate precursor and is catalyzed by linalool synthases,
80 members of the large terpene synthase gene family, and is responsible for the production of other
81 monoterpenes. Reported concentrations of linalool range from 0.01 ppm to over 0.6 ppm in fruit
82 tissue and from 1.6 ppm up to 20000 ppm in leaves[21] .

83 As a VOC, linalool plays several roles, from attraction to defense. Linalool is a major
84 constituent of the floral scent of many species and is widely used to attract pollinators, which
85 rely on sensory cues to find suitable hosts[31], and as a cue for nearby plants, informing them of
86 environmental conditions [27]. Linalool also acts as a direct defense mechanism against pathogens.
87 For example, in *Pseudomonas fluorescens,* linalool reduces membrane potential, increases
88 cellular leakage, and decreases protein content [28]. Similar modes of action have been observed in
89 fungal pathogens, including *Candida*[33], and *B. cinerea*. Specifically, Xu et al. reported that when
90 exposed to linalool, a *B. cinerea* strain downregulates ergosterol biosynthesis genes and
91 upregulates genes encoding CYP450 enzymes, a large and diverse family of enzymes involved in
92 xenobiotic detoxification, specialized metabolism, and lipid modification. Reduced ergosterol
93 biosynthesis compromises plasma membrane integrity, disrupting membrane-associated
94 signaling processes and membrane structure, as ergosterol is a vital component of the fungal
95 plasma membrane. In addition to enzymatic detoxification, other studies have identified major
96 facilitator superfamily transporters (MFS) as key components of resistance and virulence in *B.*
97 *cinerea.* These transporters mediate the efflux of toxic compounds from the cell, reducing the
98 accumulation of plant defensive SMs or other pesticides. Beyond its direct effects on pathogens,

99 linalool also acts indirectly by stimulating plant-host hormonal pathways. When *Orzo sativa* was
100 exposed to linalool, it upregulated defense genes and demonstrated enhanced resistance to the
101 bacterial pathogen *Xanthomonas oryzae*[58].
102 While there is a large support for the direct and indirect effects of linalool on plant
103 pathogen interactions, most studies focus on a single or a few isolates [53,65]. Although these
104 approaches provide valuable mechanistic insight, they capture only an individual genotype's
105 response and do not necessarily reflect how individuals across a genetically diverse population
106 respond or the strategies they employ. Given the polygenic architecture of virulence in *B. cinerea*
107 and high effective population size[13], this suggests that candidate genes for linalool resistance
108 validated in the model isolate of *B. cinerea* (BO5.10)[65] may not capture the full diversity of
109 resistance mechanisms employed across the species. While genome-wide association studies
110 (GWAS) have been successfully applied to virulence traits, few studies have examined the
111 genetic architecture of *B. cinerea's* responses to common specialized metabolites at the
112 population level [18]. To address this gap, we exposed a population *of B. cinerea* isolates to
113 linalool to assess population-level variation in resistance and to investigate underlying trait
114 genetic architecture.
115

116 **MATERIALS AND METHODS:**

117 *Botrytis Collection:*

118 We leveraged 83 isolates of the haploid *B. cinerea* association mapping population previously
119 described by Atwell et al., 2015, 2018 and Caseys et al., 2021) . Isolates were obtained from
120 more than 14 different plant species, of which 90% were isolated in California, and 10% were
121 worldwide strains regularly used for functional genomic studies [3,60]. Within this population, there

122 is little evidence of host specialization or local population structure, as Casey et al. found Fst
123 values of 0.03 between strains isolated in Europe and California, and 0.02 among isolates from
124 different plant host species [14]. All strains used in this study have been previously whole-genome
125 sequenced to an average of 164-fold coverage[5,14] and aligned to the genome assembly of B05.10
126 ASM83294v1[60] , resulting in 217,749 SNPs with a minor allele frequency greater than 0.20.

127 *Linalool Exposure:*

128 The isolates used in this study were grown for 2 weeks on oatmeal agar plates. Conidia
129 were collected from full grown plates using sterile water, counted using an automated spore
130 counter pipeline(https://github.com/melaniemadrigal07/Post.ImageProcessing) and diluted to a
131 final concentration of 10 spores/µL in a gamborg B5 (Sigma Aldrich, St. Louis MO)
132 supplemented with 41 g/L fructose (Thermo Fisher Scientific, Waltham, Massachusetts) 26.65
133 g/L glucose (Sigma Aldrich, St. Louis MO), 1.03 g/L sucrose (Fisher Scientific, Pittsburgh, PA),
134 with pH adjusted to 6.5 using 0.01 KOH. To prevent spore germination, spores were kept on ice
135 from collection to inoculation. 10 µL of the spore suspension (10 spores/µL) were inoculated
136 into a 96-well plate with 70 µL of liquid Gamborg B5, 10 µL of 1000 µM Linalool (0.045%
137 DMSO (Sigma Aldrich, St. Louis, MO), and 10 µL of OZ blue cell viability (OZBiosciences,
138 San Diego, CA), in an 8-fold replication. The 1000 µM linalool concentration was selected based
139 on its biological relevance, as reported concentrations range from 0.06 µM to 130,000 µM in
140 fruit tissues. In line with this range, Xu et al. demonstrated minimum inhibitory concentration
141 (MIC; the lowest dose that inhibited spore germination) and fungicidal concentrations (MFC; the
142 lowest dose that inhibited mycelial growth) for *B. cinerea* (MIC=20.95 µM; MFC=2,095 µM),
143 placing 1000 µM within a physiologically meaningful window that is consistent with host-
144 derived exposure and below fungicidal thresholds.

The OZ blue cell viability assay relies on mitochondrial metabolic activity in viable cells: the blue-redox dye is taken up and reduced in the mitochondria, resulting in a detectable color change. Plates were imaged every 4 hours for 72 hours for a total of 20 time points using a Cytation Gen5 Plate (Agilent, Santa Clara, CA) coupled to a Biospa (Agilent, Santa Clara, CA). Quantitative colorimetric data were extracted from the time-lapse images for subsequent analysis of respiratory rates.

Image Analysis

The Cytation Gen5 generated approximately 336,000 images, each exported as a separate red, green, and blue (RGB) channel. To organize data for analysis, an ImageJ macro was used to group and compile images by time point for each plate, for downstream analysis. Using these images, the RGB channels were converted to the L*a*b* color space, and values were extracted using a custom Python script https://github.com/melaniemadrigal07/GWASLIN). With the L* value measuring the shift from light to dark, when L = 0, it indicates a dark appearance, and L = 100 indicates a bright appearance. The a* value quantifies the shift from green to red, with negative a* indicating green and positive a* indicating a strong red color. The b* value is a proxy for the shift from blue to yellow, with a negative b* indicating a strong blue component and a positive b* indicating a strong yellow component.

To accurately extract values from the images, a 10% L-value threshold was applied to isolate hyphal growth in each well. We then measured values external to hyphae, thereby enabling quantification of color changes in the media associated with fungal metabolic activity. After extracting the color values, background correction was performed by subtracting the average L*, a*, and b* values from blank wells (media + dye without spores) from those of experimental wells at each time point.

Metabolic Activity Quantification

Generated L*, a*, b* values were combined using the following formula to obtain an ΔE value: $\sqrt{(L_2 - L_1)^2 + (a_2 - a_1)^2 + (b_2 - {b_1}^2)}$, ΔE serves as a proxy for color change relative to the first time point. This metric was used to generate a curve representing color change over time. To capture early metabolic activity, we focused on the early germination phase by using timepoints one to five (up to 20 hours post-inoculation) for downstream analyses. During this 0-20 h window, spores initiate germination and begin forming penetrative structures[14,17] (e.g., appressoria, infection cushions). In addition to ΔE, b* values were analyzed independently, as they reflect the reduction of the resazurin dye and provide a more specific measure of redox-driven metabolic activity.

Several phenotypes were extracted from the ΔE curve (Supplementary Table 1) area under the curve and maximum ΔE. The area under the curve represents the magnitude of the color change at the early time points. Max ΔE is the value at which isolates reached their peak color change. Similarly to the phenotypes extracted from ΔE, the same was done for the b* value, which represents the shift along the blue-yellow axis, with positive values indicating yellow and negative values indicating blue. The color change range was incorporated as a phenotype to represent metabolic variation in response to linalool.

To examine the foraging strategies of the strains, hyphal network images were skeletonized using SkelPy and subsequently processed with SkelpyR to remove skeletonization artifacts [40].Network-level traits were extracted, including edge lengths, total hyphal length, number of tips, number of branches, tip fraction, and branch fraction. Total hyphal length and tip number provide measures of overall growth and active extension, while tip and branch fraction

190 capture how growth is allocated between exploratory hyphal tips and network consolidation, and
191 edge length provides information on the spatial scale of individual hyphal segments.

192 A principal component analysis (PCA) was used to summarize multivariate patterns of
193 phenotypic variation among *B. cinerea* isolates. PCA was conducted separately for structural
194 hyphal network traits and metabolic traits, using the same framework for both datasets. PCAs
195 were performed on centered and scaled trait matrices using singular value decomposition,
196 excluding traits with zero variance. K-means clustering was subsequently applied to isolate
197 eigenvectors corresponding to the first two principal components. The number of clusters was set
198 to k=2 based on inspection of the within-cluster sum of squares and the elbow method.
199 Clustering was used to summarize the major axes of phenotypic variation rather than to define
200 discrete phenotypic classes.

201 *Genome-wide Association Study*

202 To estimate the genetic architecture of resistance to linalool in *B. cinerea,* we performed
203 genome-wide association using GEMMA's univariate linear mixed model [68]. Population structure
204 and relatedness among isolates were accounted for using a centered genotype matrix in
205 GEMMA. This approach was based on the model of Zhang et al. (2010) and further adapted by
206 Dowell et al.[20] In this framework, Single Nucleotide Polymorphisms (SNPs) with a minor allele
207 frequency (MAF) of > 0.20 and < 10% missing data were retained, yielding 271,495 SNPs for
208 analyses. Due to low linkage disequilibrium in *B. cinerea*[5,8], association significance was
209 assessed using a Bonferroni correction with the family-wise error rate set at $\alpha = 0.05$ divided by
210 the number of SNPs tested[23].

211 Following GWA, we assessed linkage disequilibrium (LD) among significantly
212 associated SNPs using PLINK [46]. Pairwise LD (R^2) was calculated for SNPs within 10 kb
213 windows centered on significant SNPs to assess regional associations. SNP effect sizes and
214 standard error were calculated as the beta divided by the trait range, as *B. cinerea* is haploid [42].
215 Relative effect sizes were summed across all associated regions for each trait to estimate the
216 relative effect size of the associated genomic regions. Differences in the distribution of effect
217 sizes between metabolic and structural traits were assessed using a Wilcox rank sum test in R.
218 Regions associated with multiple traits were considered colocalized. Gene functional
219 annotations, when available, were extracted from the fungal genomic resources[9]. SNPs were
220 further classified by genomic location (coding or non-coding) and mutation type (e.g.,
221 synonymous, missense, or nonsense).

222 To prioritize associated loci for downstream interpretation, we identified lead SNPs exceeding
223 the genome-wide significance thresholds ($P < 0.05/m$, where m is the number of SNPs tested)
224 and defined associated regions using local linkage disequilibrium patterns around each lead SNP
225 (pairwise R^2 within 10 kb). Among significant regions, loci were ranked by lead SNP P-value,
226 standardized effect magnitude, and evidence of colocalization across traits. Candidate genes were
227 defined as those overlapping each region or as the nearest to the lead SNP. For candidate SNPs in
228 protein-coding genes, we assessed codon bias among synonymous SNPs by reconstructing
229 reference and alternate codons for each SNP (using SNP context, CDS position, and gene strand)
230 using a custom R script(https://github.com/melaniemadrigal07/GWASLIN). Usage was then
231 compared with the genome-wide codon usage frequencies of B05.10's reference genome [57]. All
232 analyses were conducted within the R environment[48] (R Core Team 2025, version 4.5.3).

233 *Molecular Docking*

234 To explore the potential role of identified variants that directly interact with linalool,
235 rather than via indirect effects on gene expression or the overall cellular environment, we used an
236 in-silico protein-ligand binding approach. For each protein of interest, we used D-I-TASSER[67]
237 with default settings to predict its structure. D-I-TASSER was selected due to its demonstrated
238 performance in CASP benchmarking. I-T Model confidence was assessed using the reported C-
239 score (a confidence score that estimates the quality of predicted models) and the estimated TM-
240 score (a metric for assessing the topological similarity of protein structures), and the top-ranked
241 model was used for downstream analyses. To assess the interaction of linalool with predicted
242 protein transporters, we used CaverDock [41]and AutoDock Vina to estimate the binding channel
243 for simulation, employing a blind docking approach when proteins lack previously identified and
244 validated active sites. The protein Bcin07g05680 was selected among genes with significantly
245 associated SNPs as a candidate for docking analysis because it encodes an MFS transporter and
246 lacks an identified active site. Given its association with metabolic traits, we used a blind
247 docking approach to identify potential binding sites for linalool.

248 **RESULTS**

249 *Metabolic activity*

250 Across *B. cinerea* isolates, the Area Under the Curve ΔE varied from 3.57 to 109 among
251 samples, with an average of 16.9.99 ($\pm 2.2\ SE$, supplementary Table 2). The slope from timepoint
252 5 varied from -0.01 to 2.37, with an average of 0.08 ($\pm 0.01\ SE$,Supplementary Table 2). For
253 traits related to the shift along the b* axis, the maximum blue varied from -1.15 to 24.69, with an
254 average of 4.66 ($\pm 0.65\ SE$, Supplementary Table 2). The slope of b* ranged from -0.86 to 6.40
255 among samples, with an average of 0.92 ($\pm 0.17\ SE$, Supplementary Table 2). Area under the

curve along the b axis varied from -6.47 to 79.89 among samples, with an average of 11 ($\pm 1.61\ SE$, Supplementary Table S2).

Principal component analysis (PCA) of the ΔE trajectories and blue-axis traits separated isolates along PC1 and PC2. The PC1 axis accounted for 76.3% of the total variance and captured the magnitude of the metabolic response, whereas PC2 accounted for 12.6% of the variance and described differences in response timing and the shape of the metabolic activity trajectory (Figure 1B).

Hyphal network traits

Structural traits of *B. cinerea* isolates, such as fractal dimension, varied from 0.192 to 1.44, with an average of 0.72 ($\pm 0.02\ SE$, Supplementary Table 2). The slope of the fractal dimension varied from -0.11 to 0.19, with an average of 0.05 ($\pm 0.006\ SE$, Supplementary Table S1). Area under the curve of fractal dimension ranged from 1.01 to 8.73 ($\pm 0.18\ SE$, Supplementary Table 2). Cumulative total hyphal length across the time course ranged from 778 to 144,171 µm with an average of 37,519 µm ($\pm 0.02\ SE$, Supplementary Table SX). Architectural ratios such as tip fraction ranged from 0.702 to 0.937, with an average of 0.787 ($\pm 0.02\ SE$, Supplementary Table S2). The number of branch points (locations where hyphae bifurcate) ranged from 0.37 to 403, with an average of 122 ($\pm 10.7\ SE$, Supplementary Table 2). The number of tips (proxy for active regions of the hyphal region) ranged from 4.6 to 863, with an average of 294 ($\pm\ 20.3\ SE$, Supplementary Table 2). Edges representing the connectivity of the hyphal network ranged from 2.99 to 1279, with an average of 404 ($\pm\ 67.3\ SE$, Supplementary Table 2).

277 A PCA of structural traits revealed three distinct clusters among *B. cinerea* (Figure 1C). PC1
278 accounts for 69.7% of the variance and is largely driven by connectivity-related traits (high
279 AUC, fractal dimension, tips, and edges). PC2 accounts for 12.1% of the variance and is driven
280 by growth metrics (fractal dimension, slope, and fragmentation index). A PCA of both structural
281 and metabolic traits revealed a similar pattern; PC1 explained 57.3% of the total variance, and
282 PC2 explained 17.0% (Figure 1C). PC1 was primarily associated with structural traits such as
283 tips and edges. PC2 captured secondary variation, dominated by metabolic color-shift dynamics
284 along the b* axis (Figure 1D).

285 *Genetic architecture of resistance*

286 Genome-wide association analyses using the traits as phenotypes identified 202
287 significant SNP-trait associations and 101 unique SNPs (Figure 2, Supplementary Table 3).
288 Significant SNPs were distributed across the genome, with the greatest number on chromosome
289 2 (n=15; 11 non-coding,4 coding), chromosome 8 (n=13; 12 noncoding,1 coding), chromosomes
290 4 (n=11; 3 non-coding, 8 coding) and 13 (n=11 noncoding), all remaining chromosomes
291 contained 8 or fewer significant SNPs (Figure 2, Supplementary Table 3). Of the 101 unique
292 SNPs, 78 were noncoding, 16 were coding-synonymous, and 7 were coding-missense variants.
293 Several significant SNPs were mapped within or near four genes on chromosome 7
294 (*Bcin07g05680*, *Bcin07g05230, Bcin07g05240, and Bcin07g05210*), two distributed across
295 chromosomes 2 (*Bcin02g09200 and Bcin02g05460*) and 15 (Bcin15g00890), and 3
296 (*Bcin03g06600*). Although multiple SNPs supported individual loci, overlap among traits was
297 limited (Figure 2). When present, trait overlap suggests that a shared locus may contribute to
298 multiple aspects of the linalool response.

299 Multi-trait associations were rare, with most SNPs associated with a single phenotype,
300 suggesting that most SNPs contribute to specific components of the linalool response rather than
301 broadly affecting multiple traits. Here, a pleiotropy is defined as a SNP associated with multiple
302 phenotypes. Across metabolic-activity traits (ΔE and b features), several traits shared
303 associations within/near *Bcin07g05680*, which encodes a major facilitator superfamily
304 transporter. Notably, most SNPs within this locus were synonymous mutations. Metabolic traits
305 exhibited slightly larger standardized absolute SNP effect magnitudes than structural traits
306 (median = 0.131 vs 0.127; Figure 3A). However, structural traits included substantially more
307 unique SNPs (97 vs 7) and significant SNP-trait associations (181 vs 21) (Figure 3B).

308 Of the SNPs identified, 78 mapped to non-coding regions and 23 to coding regions.
309 Within coding regions, 16 were synonymous, and 7 were missense variants (Figure 4A). 6 of the
310 missense variants mapped to Bcin04g02170, a protein kinase domain-containing protein, while
311 one variant mapped to the transcription factor Bcifm1. Within Bcin04g02170, three substitutions
312 were altered amino acid charge, and two altered amino acid size class (Supplementary Table 3).
313 Notably, one substitution changed arginine to glycine, thereby shifting from a positively charged
314 residue to a nonpolar residue. Arginine is larger and can maintain its charge, allowing stronger
315 hydrogen and electrostatic bonding, while glycine is smaller, uncharged, and has a minimal
316 hydrogen side chain, which could increase flexibility and alter glycine's substrate specificity.
317 Previous work on protein kinases has shown that hydrostatic and electrostatic balance is a major
318 determinant of kinase-substrate specificity, and that residues outside the active site can influence
319 substrate specificity through effects on protein structure and electrostatic environments[36]. The
320 final missense variant mapped to the translation initiation factor Bcifm1, which changed alanine
321 to valine. Although both amino acids are nonpolar, valine is bulkier due to its branched side

322 chain. This increase in steric volume could subtly alter local packing, protein stability, or
323 interaction surfaces[26].

324 Among synonymous SNPs, codon usage frequency varied in direction and magnitude
325 (Figure 4B). Six variants (46.2%) shifted towards rarer codons, one variant (7.7%) shifted
326 towards the preferred codon, and six variants (46.2%) shifted to codons with approximately
327 equal usage across the genome. At the gene level, synonymous hits predominantly shifted
328 toward rarer codons (6/7), suggesting a potential directional bias in codon usage changes across
329 multiple loci, with the largest magnitude change observed in *Bcin07g05680* (MFS transporter-
330 encoding gene). In contrast, *Bcin02g08180* (AP complex subunit beta) exhibited a synonymous
331 shift in which the minor allele encoded a more preferred codon relative to the major allele
332 (Figure 4B).

333 *Docking Results*

334 Bcin07g05680 was selected as a protein of interest for follow-up docking analysis, based
335 on the presence of significantly associated synonymous SNPs. This gene was selected as a
336 candidate because its functionality is expected to be conserved across the population, while its
337 expression may be more sensitive to transcriptional and/or translational variation arising from
338 codon usage differences [57]. Putative ligand transport pathways were identified using CaverWeb
339 to calculate potential access tunnels. CaverWeb generated over 232 pockets of interest. As many
340 of these predicted pathways were either shallow, discontinuous, or sterically constrained,
341 subsequent analyses focused on tunnels likely to represent physiologically relevant transport
342 routes. The primary pocket was chosen based on quantitative criteria associated with functional
343 substrate channels, such as having the widest bottleneck (2.87 $\pm$ 0.43), the shortest path (11.46 $\pm$
344 5.79), and a curvature of 1.14 ($\pm$ 0.11). These parameters suggested a more accessible path for

345 ligand transport than other tunnels.[41] Using Caverweb, linalool was docked to transport through
346 the first tunnel. Transport through this tunnel exhibited a favorable trajectory, with values
347 ranging from approximately -4.0 kcal/mol near the internal binding region to -2.6 kcal/mol as it
348 exited the pocket. This trajectory suggests a low energetic barrier for diffusion through the
349 tunnel, supporting the possibility that this transporter could facilitate the export of small,
350 lipophilic compounds such as linalool.

351 **Discussion**

352 *Phenotypic Variation*

353 Filamentous fungi exhibit substantial phenotypic plasticity in growth form and
354 metabolism in response to environmental stressors, and these responses often reflect alternative
355 strategies that balance exploration, resource acquisition, and damage mitigation[12]. In *B. cinerea,*
356 exposure to linalool revealed isolate-to-isolate variation in metabolic activity, as quantified by
357 ΔE and b* dynamics (Figure 1B). Isolates with steep ΔE slopes displayed rapid color shifts,
358 suggesting rapid metabolic activity. Isolates with gradual slopes may experience a slower
359 metabolic response or higher susceptibility to linalool toxicity. Linalool has been shown to
360 disrupt mitochondrial function and downregulate mitochondrial and ergosterol genes, as well as
361 glutathione synthesis [65], which may underlie the observed differences in ΔE trajectories.

362 These patterns were recapitulated by PCA of metabolic traits (Figure 1B). PC1 (63.8% of
363 total variance) captured response magnitude, separating isolates with higher AUC and steep ΔE
364 slopes (fast responders) from those with more gradual slopes (slow responders). PC2 (16.7%)
365 captured variation in response timing and trajectory, distinguishing isolates with earlier versus
366 later dye reduction. Although isolates formed two broad groups with minimal overlap along PC1,
367 overlap among PC2 suggests that metabolic phenotypes are better described as a continuum

368 dominated by response strength rather than discrete classes. Together, these patterns suggest that
369 isolates differ in both the strength and the rate at which they maintain metabolic reducing
370 capacity under linalool exposure, potentially reflecting variation in tolerance mechanisms.
371 Similarly, Fusarium responds to linalool exposure through broad transcriptional remodeling, with
372 enrichment in ABC transporter activity, sterol biosynthesis, and glutathione metabolism[37] ,
373 supporting a model in which linalool perturbs membrane homeostasis, detoxification, and redox
374 buffering pathways. While resistance to chemical stress can be expressed not only through
375 physiological detoxification. Filamentous fungi can also respond by reprogramming growth
376 through adjustments in hyphal tips, branching, and network connectivity to reallocate growth
377 under inhibitory conditions. In *Rhizophagus irregularis,* exposure to fungicides reduces hyphal
378 length and alters anastomosis, demonstrating that chemical environments can reshape hyphal
379 architecture and interaction behavior [49]

380 Isolates not only differ in metabolic activity but also in structural traits, reflecting
381 differences in how each isolate's hyphal network responds to linalool (Figure 1A). Network
382 features, such as fractal dimension, hyphal tips, and edges, varied across the population,
383 reflecting differences in network complexity and connectivity (Supplementary Table 1). These
384 traits reveal that some isolates form compact, highly interconnected networks, whereas others
385 exhibit more of an exploratory phenotype. In the structural PCA (Figure 1A), isolates are
386 separated into three broad morphological groupings driven by network size and connectivity
387 metrics (edges, nodes, tips, branches, and total hyphal length). Similar contrasts have been
388 described in filamentous fungi under different environmental conditions, where dense, cohesive
389 networks are associated with nutrient-rich environments and exploratory growth with nutrient-
390 poor environments [2,22]. In the context of linalool, one possibility is that highly connected

391 networks increase physiological robustness (i.e., maintaining growth by distributing transport
392 and reducing power demands across a denser mycelial system), while exploratory architectures
393 reflect avoidance or slower growth under stronger inhibition. More broadly, the observed
394 architectural plasticity aligns with evidence that *B. cinerea* can undergo hyphal specialization as
395 a strategy to overcome host defenses[47]. Infection cushions, specialized multicellular structures
396 that secrete cell wall-degrading enzymes, exhibit higher tolerance to host defenses[47]. The
397 structural diversity we observe may mirror this, suggesting that remodeling of the hyphal
398 network is a key in *B. cinerea's* ability to overcome host defenses and enact disease.

399 *Genetic Architecture of Resistance to Linalool*

400 Linalool exposure is known to elicit broad physiological remodeling in *B. cinerea,*
401 including disruption of mitochondrial function and changes in sterol and redox processes[37,65]. In
402 a proteomic time course, brief exposure to linalool led to broad proteomic changes, involving
403 enrichment of proteins involved in translation, amino acid metabolism, and post-translational
404 modification[65]. These findings suggest that linalool triggers energetic and metabolic
405 reprogramming in response to mitochondrial stress and membrane disruption.

406 In our GWAS, the strongest metabolic response associations localized to *Bcin07g05680*,
407 an MFS transporter-encoding gene. Most of these variants were synonymous, indicating no
408 change in the amino acid sequence; however, this mutation could influence protein expression or
409 conformation via mRNA stability or translation efficiency[1]. This mechanism has been
410 demonstrated in the multidrug resistance gene MDR1, where a synonymous polymorphism
411 altered substrate specificity by altering folding and drug-protein interactions[34] . The synonymous
412 mutations in *Bcin07g05680* resulted in shifts toward the use of non-preferred or uncommon
413 codons (Figure 4B). Importantly, codon usage mismatch has been shown to have strong

414 functional consequences in *B. cinerea*[57]. Codon optimization of the geneticin resistance gene
415 NPTII to match *B. cinerea* codon preferences increases transformation by 30-fold, demonstrating
416 that *B. cinerea* is sensitive to codon usage in heterologous coding sequences[57]. While a shift
417 toward rarer codons could be detrimental under baseline conditions due to reduced translational
418 efficiency, the net fitness effect of these synonymous changes may be context-dependent and
419 could be favored under linalool exposure[43]. In *Salmonella,* codon usage bias has been linked to
420 stress and virulence-associated gene regulation, where enrichment towards synonymous codons
421 is thought to support translation under nutrient-limited conditions and allows for colonization of
422 different host tissues[11].

423 Efflux transporters are frequently implicated in chemical stress responses in fungal
424 pathogens. In Fusarium, a GWAS examining sensitivity to the demethylation inhibitor (DMI)
425 class of fungicides identified candidate loci mapping to transport-related proteins [56], suggesting
426 that membrane transport is part of a broader genetic toolkit to cope with chemical-related stress.
427 In *B. cinerea,* for example, transcriptomic comparisons of fludioxonil-resistant isolates found
428 MFS to be upregulated in fludioxonil-resistant isolates [38]. In addition, the *MfsG* transporter has
429 been identified as a virulence factor that confers tolerance to other SMs, such as glucosinolates[61].
430 To explore whether this transporter could interact with linalool, molecular docking was
431 performed using the predicted *Bcin07g05680* (MFS transporter) protein structure. Notably, the
432 variants in/near *Bcin07g05680* (MFS transporter) *were* predominantly synonymous and shifted
433 codon usage toward rarer codons, providing a plausible translation-linked route by which silent
434 variation could influence transporter performance. In addition, *Bcin07g05210,* a btb domain-
435 containing protein, was associated with variation in metabolic response, suggesting a potential
436 regulatory role in mediating cellular adaptation to linalool exposure.

437 Several SNPs were linked to variation in structural traits, including the area under the
438 fractal dimension curve, total hyphal length, and tip fraction (Figure 2). These traits capture
439 differences in hyphal network connectivity and cohesion. Associated loci were in a mitochondrial
440 translation initiation factor (*Bcin02g09200*), a Zn-C6 domain containing protein
441 (*Bcin02g05460*), *Bcin02g08180* (AP complex subunit beta), and *bcltf1*. *Bcin02g09200* may
442 contribute to variation in hyphal structure by regulating mitochondrial efficiency and availability.
443 As hyphae extend and grow, the hyphal tips rely on ATP for growth; therefore, small shifts in
444 mitochondrial activity could alter branching frequency and overall network cohesion. The ZN(II)
445 C6 domain-containing transcription factor (Bcin02g05460) is likely to regulate downstream
446 genes involved in carbon metabolism, stress signaling, and cell wall synthesis. In other
447 filamentous fungi, ZN(II) C6 proteins regulate carbon metabolism and drug sensitivity [39].
448 *Bcin02g08180* encodes an AP complex subunit beta, which is involved in vesicle-mediated
449 trafficking and cargo sorting. Vesicle trafficking is critical for fungal virulence in *B. cinerea* as it
450 transports sRNAs to plants via extracellular vesicles[30]. Extracellular vesicles carry a diverse set
451 of cargo that range from involvement in transport to autophagy[19]. *Bcltf1* has been categorized as
452 a transcription factor that regulates virulence, with deletion mutants exhibiting hypersensitivity
453 to oxidative stresses, therefore variation within *Bcltf1* could plausibly influence responses to
454 oxidative stress from linalool exposure[52].

455 Our *B. cinerea* population showed that in response to linalool exposure, phenotypic
456 diversity is driven by metabolic and morphological plasticity. At the population level, metabolic
457 resistance to linalool appears to be governed by a small number of genes, suggesting an
458 oligogenic basis for this trait. This pattern contrasts with prior studies showing that variation in
459 *B. cinerea* virulence and host is polygenic, involving many loci of small effect that shape lesion

460 formation and host specificity [7,14,51,54,55]. Correlation of lesion areas across different hosts
461 highlights that virulence is driven by hundreds of genes scattered throughout the genome [6,14,55].
462 In contrast, resistance to specific host-derived defenses, such as linalool, may be mediated by a
463 smaller set of key genes, such as transporters with broad substrate specificity or stress response
464 regulators that can exert larger individual effects on survival and growth under chemical
465 challenge. Consistent with this, experimental evolution with specialized metabolites can induce
466 multidrug resistance in *B. cinerea* via upregulation of ABC and MFS transporter genes [64].
467 Additionally, work in a Michigan *B. cinerea* population found that fungicide resistance was
468 consistently associated with detectable population differentiation, supporting the idea that
469 chemical exposure can act as a strong selective pressure and shape the genetic architecture of
470 resistance in the *B. cinerea* population[45] .

471 These results provide insight into how *B. cinerea* overcomes host defenses and how it
472 functions with known virulence mechanisms, demonstrating that its success as a generalist
473 pathogen arises from a mixed genetic architecture that balances a polygenic basis for virulence
474 with oligogenic resistance mechanisms to linalool. While our study is one of the first to examine
475 a population of *B. cinerea* response to linalool, our population represents a subset of the total
476 genetic diversity and may not capture all allelic variation underlying resistance. Moreover, the
477 population was tested against a single VOC, whereas during natural host-pathogen interactions,
478 *B. cinerea* encounters mixtures of hundreds of specialized metabolites. Future work should
479 incorporate broader isolate sampling and exposure to mixtures of specialized metabolites, which
480 is necessary to elucidate the full genetic architecture of resistance.

481

482 **Data Availability Statement**

All code used for image processing and downstream analyses is available at . (https://github.com/melaniemadrigal07/GWASLIN). Supplementary material is available at 10.5281/zenodo.19425171and provides detailed information supporting the analyses performed in this study. Supplementary Table 1 provides descriptions of the traits used in this study. Supplementary Table 2 contains trait means. Supplementary Table 3 contains results of the genome wide association analyses it includes SNPs, genomic positions, effect sizes, and statistically significant values for all trait-SNP associations. Supplementary Table 4 provides descriptions of all annotation fields used in SNP characterization including genomic location, allele identity, codon context, and functional classification. Supplementary Table 5 contains location of the SNP and classification of the mutation.

Acknowledgments

J.A.D., M.M., and J.C.M. were funded in part by a USDA grant (2022-67012-43019). M.M. was also funded by the Future Scholar fellowship at Louisiana State University.

M.M. and J.A.D. designed the study; M.M. and J.C.M. collected the data; M.M, J.C.M., and J.A.D. analyzed the data; and M.M. and J.A.D. wrote the manuscript with input from D.J.K. and J.C.M.

Study funding

J.D., M.M., and J.M. were funded in part by a USDA grant (2022-67012-43019). M.M. was also funded by the Future scholar's fellowship at Louisiana State University.

Conflict of interest

None declared.

508 **Figures**

509

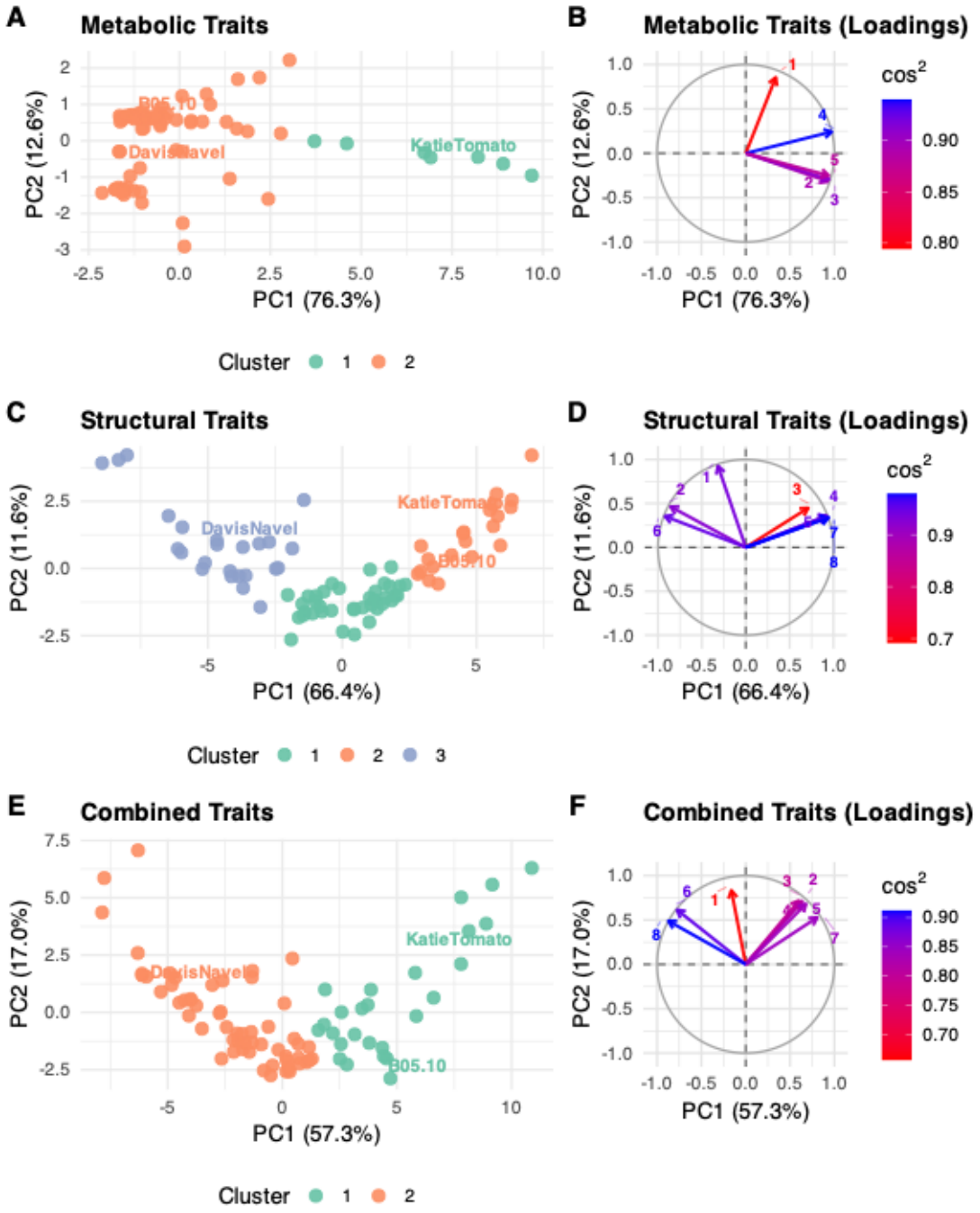

510

511 **Figure 1. Metabolic and structural trait variation across isolates** (A, C, E): PCA score plots
512 of *B. cinerea* isolates projected onto PC1 and PC2 for metabolic (A), structural (C), and
513 combined (E) trait datasets. Points are colored by k-means cluster assignment (k=3 for structural,
514 2 for metabolic, and combined), selected isolates are labeled for reference, including B05.10

(reference and generalist isolate), KatieTomato (highly virulent isolate), DavisNavel (low virulent isolate). (B, D, F) Corresponding loading plots displaying the top contributing traits for each dataset. Arrows represent variable loadings on PC1 and PC2. In (B), Traits in numerical order: 1, time point of maximum blue axis shift; 2, maximum delta E at timepoint 5 (20 hpi); 3, area under the curve at timepoint 5 (20 hpi); 4 slope of blue axis shift at timepoint 5 (20 hpi); 5 slope of delta E at timepoint 5. (D) Traits in numerical order: 1, tip fraction residuals; 2, weighted tip fractions; 3, area under the curve of fractal dimension across 72 hours; 4, total hyphal length; 5, mean total hyphal length; 6, median edge length; 7, number of hyphal tips; 8, number of hyphal nodes. (F) 1, tip fraction residuals; 2, maximum blue axis shift; 3, range of blue axis; 4 slope of blue axis shift at timepoint 5 (20 hpi); 5, area under the curve of blue axis at timepoint 5 (20 hpi); 6, tip fraction weighted; 7, area under the curve of delta eat timepoint 5 (20 hpi) 8, median edge length.

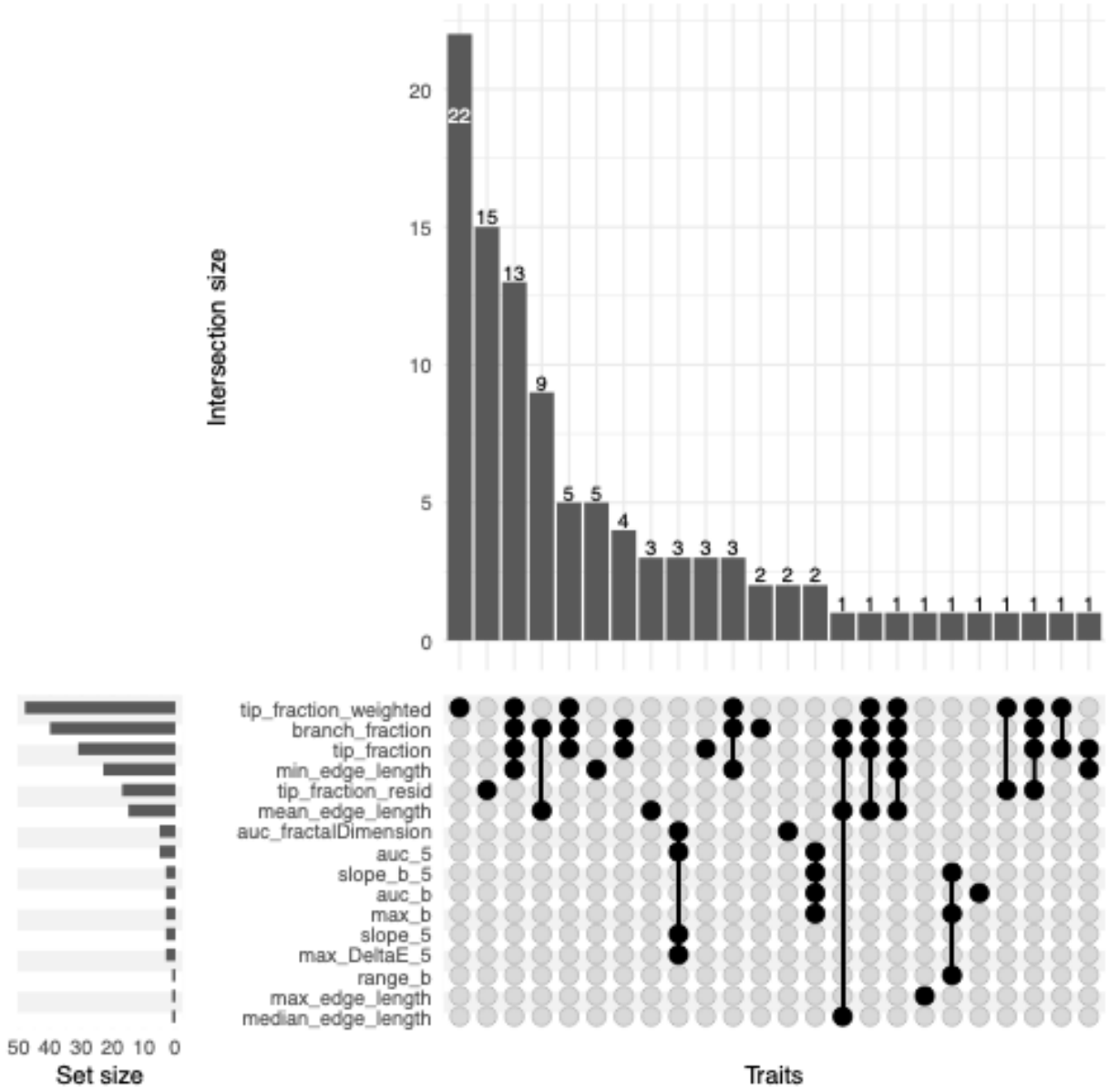

Figure 2. Overlap of significant SNPs and trait associations.

Upset plot showing the intersection of significant SNPs across measured traits. Vertical bars represent the number of SNPs shared among specific combination of traits (intersection size). Horizontal bars indicate the total number of SNPs associated with each individual trait (set size) Connected black dots denote traits included in each intersection.

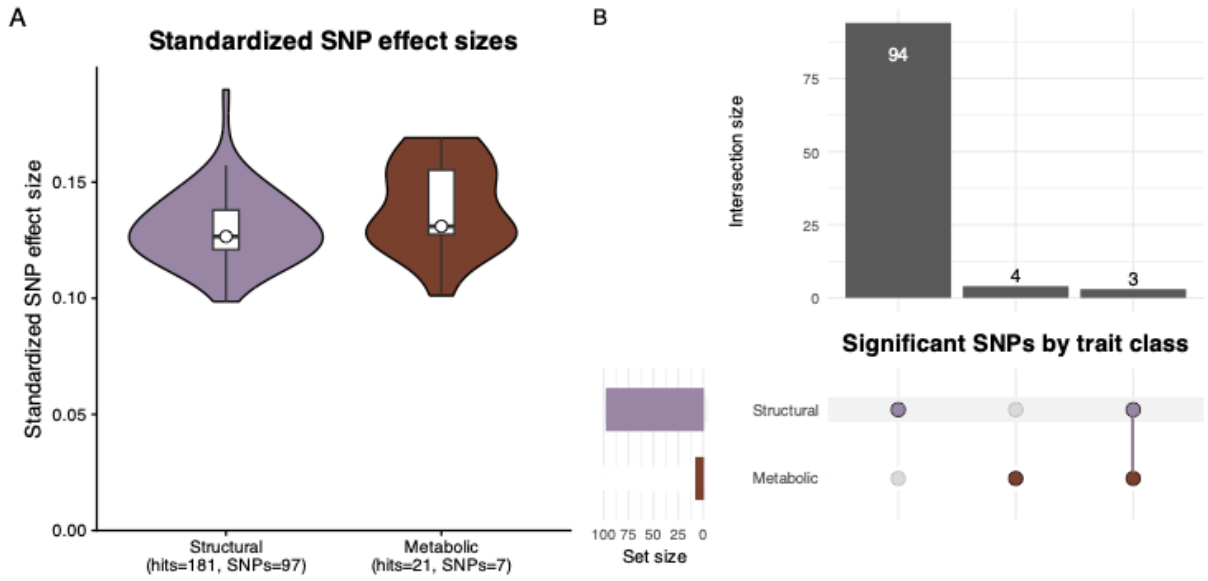

Figure 3. Distribution and overlap of significant SNP associations across structural and metabolic trait classes. A) Distribution of standardized SNP effect sizes for structural and metabolic traits (Wilcox rank sum test=1233, P<0.01). Violins represent the full distribution of absolute effect sizes across significant SNP-trait associations, and boxplots indicate the interquartile range and median. Sample sizes (total significant associations and unique SNPs are shown below each category. Hits refer to significant SNP-trait associations, while SNP counts represent unique variants after collapsing repeated associations across traits. (B) Upset plot showing the number of unique SNPs associated with structural traits, metabolic traits, or both. Vertical bars represent interaction sizes, and the matrix below indicates the trait class for each intersection. Structural SNPs account for the most significant associations, with limited overlap between structural and metabolic traits.

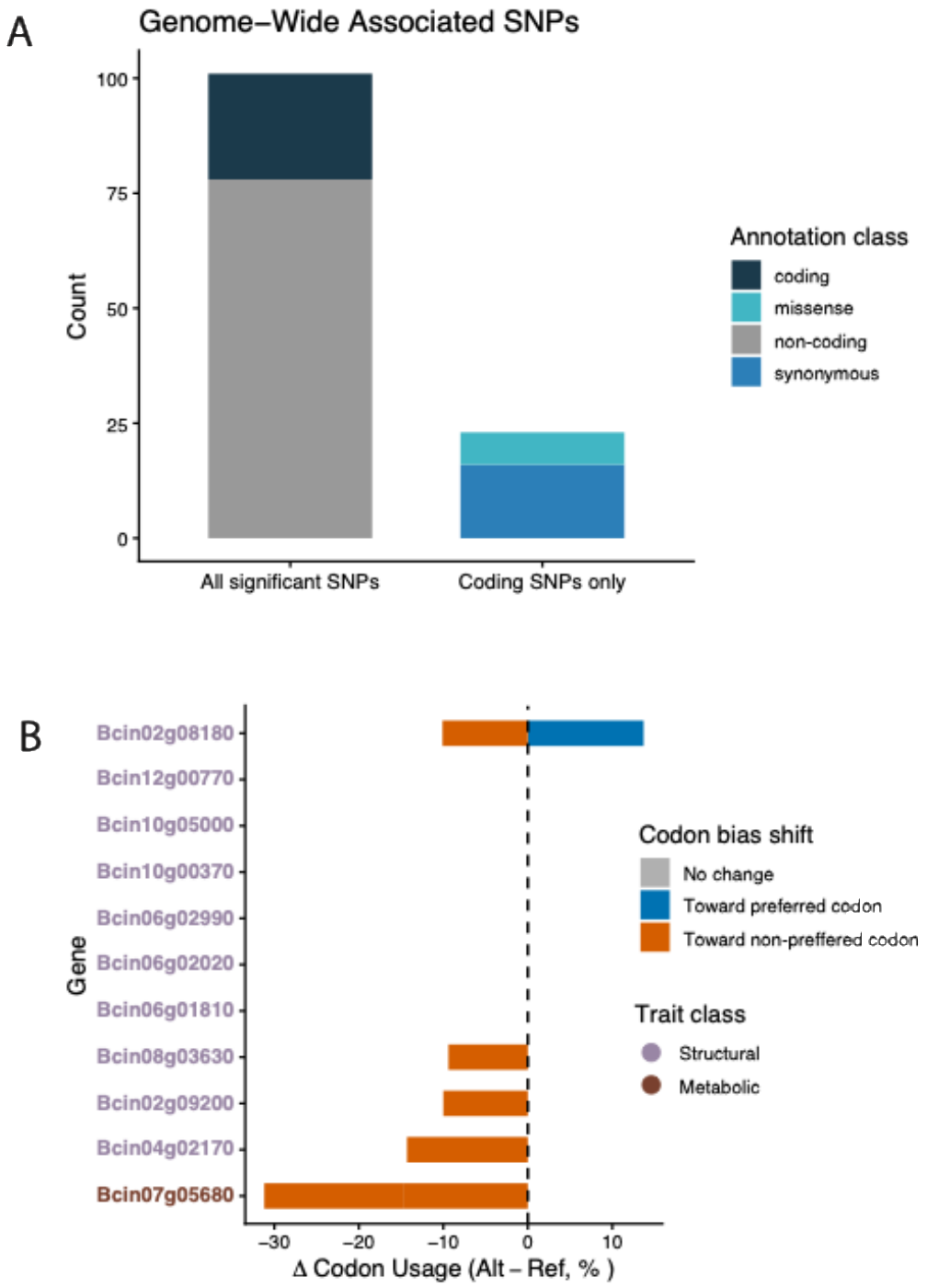

547

548 **Figure 4. Functional annotation and codon bias shifts among genome-wide significant**
549 **SNPs.** (A) Distribution of genome-wide associated SNPs partitioned into coding and non-coding

categories. Coding SNPs are further subdivided into synonymous or missense variants. (B) Change in codon usage bias for synonymous SNPs in coding regions between the alternate and reference alleles. Positive values indicate shifts toward more preferred codons, whereas negative values indicate shifts towards non-preferred codons. Colors denote the direction of change, and gene labels indicate the trait class.

References

1. A “Silent” Polymorphism in the MDR1 Gene Changes Substrate Specificity | Science. [accessed 2026 Jan 17]. https://www-science-org.libezp.lib.lsu.edu/doi/10.1126/science.1135308

2. Aguilar-Trigueros CA, Boddy L, Rillig MC, Fricker MD. Network traits predict ecological strategies in fungi. ISME Communications. 2022;2(1):1–11. doi:10.1038/s43705-021-00085-1

3. Amselem J, Cuomo CA, Couloux A, Coutinho PM, de Vries RP, Dyer PS, Fillinger S, Gout L, Hahn M, Kohn L, et al. Genomic Analysis of the Necrotrophic Fungal Pathogens Sclerotiniasclerotiorum and Botrytiscinerea.

4. Aprotosoaie AC, Hăncianu M, Costache I-I, Miron A. Linalool: a review on a key odorant molecule with valuable biological properties. Flavour and Fragrance Journal. 2014;29(4):193–219. doi:10.1002/ffj.3197

5. Atwell S, Corwin J, Soltis N, Subedy A, Denby K, Kliebenstein DJ. Whole genome resequencing of Botrytis cinerea isolates identifies high levels of standing diversity. Frontiers in Microbiology. 2015 [accessed 2026 Jan 18];6.

https://www.frontiersin.org/journals/microbiology/articles/10.3389/fmicb.2015.00996/full. doi:10.3389/fmicb.2015.00996

6. Atwell S, Corwin J, Soltis N, Subedy A, Denby K, Kliebenstein DJ. Whole genome resequencing of Botrytis cinerea isolates identifies high levels of standing diversity. Frontiers in Microbiology. 2015 [accessed 2025 Sept 1];6. https://www.frontiersin.org/journals/microbiology/articles/10.3389/fmicb.2015.00996/full. doi:10.3389/fmicb.2015.00996

7. Atwell S, Corwin JA, Soltis N, Zhang W, Copeland D, Feusier J, Eshbaugh R, Kliebenstein DJ. Resequencing and association mapping of the generalist pathogen *Botrytis cinerea*. 2018 [accessed 2024 Sept 14]. http://biorxiv.org/lookup/doi/10.1101/489799. doi:10.1101/489799

8. Atwell S, Corwin JA, Soltis N, Zhang W, Copeland D, Feusier J, Eshbaugh R, Kliebenstein DJ. Resequencing and association mapping of the generalist pathogen *Botrytis cinerea*. 2018 [accessed 2024 Sept 10]. http://biorxiv.org/lookup/doi/10.1101/489799. doi:10.1101/489799

9. Basenko EY, Pulman JA, Shanmugasundram A, Harb OS, Crouch K, Starns D, Warrenfeltz S, Aurrecoechea C, Stoeckert CJ, Kissinger JC, et al. FungiDB: An Integrated Bioinformatic Resource for Fungi and Oomycetes. Journal of Fungi. 2018;4(1):39. doi:10.3390/jof4010039

10. Blande JD, Holopainen JK, Li T. Air pollution impedes plant-to-plant communication by volatiles. Ecology Letters. 2010;13(9):1172–1181. doi:10.1111/j.1461-0248.2010.01510.x

11. Bumann D. tRNA modifications enable codon usage signatures to coordinate bacterial virulence in Salmonella.

12. Camenzind T, Aguilar-Trigueros CA, Hempel S, Lehmann A, Bielcik M, Andrade-Linares DR, Bergmann J, Dela Cruz J, Gawronski J, Golubeva P, et al. Towards establishing a fungal economics spectrum in soil saprobic fungi. Nature Communications. 2024;15(1):3321. doi:10.1038/s41467-024-47705-7

13. Caseys C, Shi G, Soltis N, Gwinner R, Corwin J, Atwell S, Kliebenstein D. Quantitative interactions drive *Botrytis cinerea* disease outcome across the plant kingdom. 2018 [accessed 2025 Dec 12]. http://biorxiv.org/lookup/doi/10.1101/507491. doi:10.1101/507491

14. Caseys C, Shi G, Soltis N, Gwinner R, Corwin J, Atwell S, Kliebenstein DJ. Quantitative interactions: the disease outcome of Botrytis cinerea across the plant kingdom. G3: Genes|Genomes|Genetics. 2021;11(8):jkab175. doi:10.1093/g3journal/jkab175

15. Catola S, Centritto M, Cascone P, Ranieri A, Loreto F, Calamai L, Balestrini R, Guerrieri E. Effects of single or combined water deficit and aphid attack on tomato volatile organic

compound (VOC) emission and plant-plant communication. Environmental and Experimental Botany. 2018;153:54–62. doi:10.1016/j.envexpbot.2018.05.001

16. Cellini A, Biondi E, Blasioli S, Rocchi L, Farneti B, Braschi I, Savioli S, Rodriguez-Estrada M t., Biasioli F, Spinelli F. Early detection of bacterial diseases in apple plants by analysis of volatile organic compounds profiles and use of electronic nose. Annals of Applied Biology. 2016;168(3):409–420. doi:10.1111/aab.12272

17. Choquer M, Rascle C, Gonçalves IR, de Vallée A, Ribot C, Loisel E, Smilevski P, Ferria J, Savadogo M, Souibgui E, et al. The infection cushion of Botrytis cinerea: a fungal 'weapon' of plant-biomass destruction. Environmental Microbiology. 2021;23(4):2293–2314. doi:10.1111/1462-2920.15416

18. Corwin JA, Subedy A, Eshbaugh R, Kliebenstein DJ. Expansive Phenotypic Landscape of *Botrytis cinerea* Shows Differential Contribution of Genetic Diversity and Plasticity. Molecular Plant-Microbe Interactions®. 2016;29(4):287–298. doi:10.1094/MPMI-09-15-0196-R

19. De Vallée A, Dupuy J-W, Moriscot C, Gallet B, Vanderperre S, Guignard G, Rascle C, Calvar G, Malbert B, Gillet F-X, et al. Extracellular Vesicles of the Plant Pathogen Botrytis cinerea. Journal of Fungi. 2023;9(4):495. doi:10.3390/jof9040495

20. Dowell JA, Bowsher AW, Jamshad A, Shah R, Burke JM, Donovan LA, Mason CM. Historic breeding practices contribute to germplasm divergence in leaf specialized metabolism and ecophysiology in cultivated sunflower (Helianthus annuus). American Journal of Botany. 2024;111(11):e16420. doi:10.1002/ajb2.16420

21. Duke JA. Handbook of phytochemical constituents of GRAS herbs and other economic plants. Boca Raton: CRC Press; 2001. (Herbal reference library).

22. Fricker MD, Heaton LLM, Jones NS, Boddy L. The Mycelium as a Network. Microbiology Spectrum. 2017;5(3):10.1128/microbiolspec.funk-0033–2017. doi:10.1128/microbiolspec.funk-0033-2017

23. Gao X, Starmer J, Martin ER. A multiple testing correction method for genetic association studies using correlated single nucleotide polymorphisms. Genetic Epidemiology. 2008;32(4):361–369. doi:10.1002/gepi.20310

24. Garagounis C, Delkis N, Papadopoulou KK. Unraveling the roles of plant specialized metabolites: using synthetic biology to design molecular biosensors. New Phytologist. 2021;231(4):1338–1352. doi:10.1111/nph.17470

25. Goh H-H, Khairudin K, Sukiran NA, Normah M n., Baharum S n. Metabolite profiling reveals temperature effects on the VOCs and flavonoids of different plant populations. Plant Biology. 2016;18(S1):130–139. doi:10.1111/plb.12403

26. Gregoret LM, Sauer RT. Tolerance of a protein helix to multiple alanine and valine substitutions. Folding and Design. 1998;3(2):119–126. doi:10.1016/S1359-0278(98)00017-0

27. Guo D, Liu Z, Raaijmakers JM, Xu Y, Yang J, Erb M, Zhang J, Zhu Y-G, Xu J, Hu L. Linalool-triggered plant-soil feedback drives defense adaptation in dense maize plantings. Science. 2025;389(6761):eadv6675. doi:10.1126/science.adv6675

28. Guo F, Chen Q, Liang Q, Zhang M, Chen W, Chen H, Yun Y, Zhong Q, Chen W. Antimicrobial Activity and Proposed Action Mechanism of Linalool Against Pseudomonas fluorescens. Frontiers in Microbiology. 2021 [accessed 2025 Sept 14];12. https://www.frontiersin.org/journals/microbiology/articles/10.3389/fmicb.2021.562094/full. doi:10.3389/fmicb.2021.562094

29. Hammerbacher A, Coutinho TA, Gershenzon J. Roles of plant volatiles in defence against microbial pathogens and microbial exploitation of volatiles. Plant, Cell & Environment. 2019;42(10):2827–2843. doi:10.1111/pce.13602

30. He B, Wang H, Liu G, Chen A, Calvo A, Cai Q, Jin H. Fungal small RNAs ride in extracellular vesicles to enter plant cells through clathrin-mediated endocytosis. Nature Communications. 2023;14(1):4383. doi:10.1038/s41467-023-40093-4

31. Heuel KC, Raguso RA, Coogan E, Mallick R, Keleher KJ, Ayasse M, Gegear RJ, Burger H. Spatial partitioning of floral volatiles provides a “chemosensory roadmap” for bumblebee pollinators. Current Biology. 2025;35(7):1622-1630.e6. doi:10.1016/j.cub.2025.02.010

32. Junker RR, Kuppler J, Amo L, Blande JD, Borges RM, van Dam NM, Dicke M, Dötterl S, Ehlers BK, Etl F, et al. Covariation and phenotypic integration in chemical communication displays: biosynthetic constraints and eco-evolutionary implications. New Phytologist. 2018;220(3):739–749. doi:10.1111/nph.14505

33. Khan A, Ahmad A, Akhtar F, Yousuf S, Xess I, Khan LA, Manzoor N. Ocimum sanctum essential oil and its active principles exert their antifungal activity by disrupting ergosterol biosynthesis and membrane integrity. Research in Microbiology. 2010;161(10):816–823. doi:10.1016/j.resmic.2010.09.008

34. Kimchi-Sarfaty C, Oh JM, Kim I-W, Sauna ZE, Calcagno AM, Ambudkar SV, Gottesman MM. A “Silent” Polymorphism in the *MDR* 1 Gene Changes Substrate Specificity. Science. 2007;315(5811):525–528. doi:10.1126/science.1135308

35. de Lacy Costello BPJ, Adamatzky AI. Assessing the chemotaxis behavior of Physarum polycephalum to a range of simple volatile organic chemicals. Communicative & Integrative Biology. 2013;6(5):e25030. doi:10.4161/cib.25030

36. Li L, Shakhnovich EI, Mirny LA. Amino acids determining enzyme-substrate specificity in prokaryotic and eukaryotic protein kinases. Proceedings of the National Academy of Sciences. 2003;100(8):4463–4468. doi:10.1073/pnas.0737647100

37. Li X, Wang Q, Li H, Wang X, Zhang R, Yang X, Jiang Q, Shi Q. Revealing the Mechanisms for Linalool Antifungal Activity against Fusarium oxysporum and Its Efficient Control of Fusarium Wilt in Tomato Plants. International Journal of Molecular Sciences. 2022;24(1):458. doi:10.3390/ijms24010458

38. Liu M, Peng J, Wang X, Zhang W, Zhou Y, Wang H, Li X, Yan J, Duan L. Transcriptomic Analysis of Resistant and Wild-Type Botrytis cinerea Isolates Revealed Fludioxonil-Resistance Mechanisms. International Journal of Molecular Sciences. 2023;24(2):988. doi:10.3390/ijms24020988

39. MacPherson S, Larochelle M, Turcotte B. A Fungal Family of Transcriptional Regulators: the Zinc Cluster Proteins. Microbiology and Molecular Biology Reviews. 2006;70(3):583–604. doi:10.1128/MMBR.00015-06

40. Madrigal M, Moseley AJ, Moseley JC, Dowell JA. SkelPy: A graphic user interface–based approach for skeletonizing fungal networks. Applications in Plant Sciences. n/a(n/a):e70049. doi:10.1002/aps3.70049

41. Marques SM, Borko S, Vavra O, Dvorsky J, Kohout P, Kabourek P, Hejtmanek L, Damborsky J, Bednar D. Caver Web 2.0: analysis of tunnels and ligand transport in dynamic ensembles of proteins. Nucleic Acids Research. 2025;53(W1):W132–W142. doi:10.1093/nar/gkaf399

42. Masalia RR, Temme AA, Torralba N de leon, Burke JM. Multiple genomic regions influence root morphology and seedling growth in cultivated sunflower (Helianthus annuus L.) under well-watered and water-limited conditions. PLOS ONE. 2018;13(9):e0204279. doi:10.1371/journal.pone.0204279

43. McInerney JO. 1 Genomic Perplexity and the Evolution of Context-Dependent 2 Function.

44. Muhich AJ, Singh R, Tom C, Caseys C, Srinivas K, Faieta L, Grabbe B, Kliebenstein DJ. Host-Botrytis co-transcriptomics reveals finely tuned interactions with closely related legumes. 2026 [accessed 2026 Apr 2]:2026.01.20.700702. https://www.biorxiv.org/content/10.64898/2026.01.20.700702v1. doi:10.64898/2026.01.20.700702

45. Naegele RP, DeLong J, Alzohairy SA, Saito S, Abdelsamad N, Miles TD. Population Genetic Analyses of Botrytis cinerea Isolates From Michigan Vineyards Using a High-Throughput Marker System Approach. Frontiers in Microbiology. 2021;12:660874. doi:10.3389/fmicb.2021.660874

46. Purcell S, Neale B, Todd-Brown K, Thomas L, Ferreira MAR, Bender D, Maller J, Sklar P, De Bakker PIW, Daly MJ, et al. PLINK: A Tool Set for Whole-Genome Association and Population-Based Linkage Analyses. The American Journal of Human Genetics. 2007;81(3):559–575. doi:10.1086/519795

47. Qian C, Lin Y, Zhu C, Liu H, Zhao J, Li X, Ren D, Li J, Wang Y, Xu L, et al. Dynamic hyphal specialization remodeling enables Botrytis cinerea to overcome diverse host defenses during infection. Physiological and Molecular Plant Pathology. 2025 Sept:102966. doi:10.1016/j.pmpp.2025.102966

48. R Core Team. R: A Language and Environment for Statistical Computing. Vienna, Austria: R Foundation for Statistical Computing; 2025. https://www.R-project.org/

49. Rodriguez-Morelos VH, Calonne-Salmon M, Declerck S. Anastomosis within and between networks of Rhizophagus irregularis is differentially influenced by fungicides. Mycorrhiza. 2023;33(1–2):15–21. doi:10.1007/s00572-023-01103-x

50. Rowe HC, Kliebenstein DJ. Complex Genetics Control Natural Variation in *Arabidopsis thaliana* Resistance to *Botrytis cinerea*. Genetics. 2008;180(4):2237–2250. doi:10.1534/genetics.108.091439

51. Rowe HC, Kliebenstein DJ. Elevated Genetic Variation Within Virulence-Associated *Botrytis cinerea* Polygalacturonase Loci. Molecular Plant-Microbe Interactions®. 2007;20(9):1126–1137. doi:10.1094/MPMI-20-9-1126

52. Schumacher J, Simon A, Cohrs KC, Viaud M, Tudzynski P. The Transcription Factor BcLTF1 Regulates Virulence and Light Responses in the Necrotrophic Plant Pathogen Botrytis cinerea. PLOS Genetics. 2014;10(1):e1004040. doi:10.1371/journal.pgen.1004040

53. Shen Q, Li H, Wang Q, Wang J, Ge J, Yang X, Wang X, Li X, Zhang Y, Zhang R, et al. Alleviating Effects of Linalool Fumigation on Botrytis cinerea Infections in Postharvest Tomato Fruits. Horticulturae. 2022;8(11):1074. doi:10.3390/horticulturae8111074

54. Singh R, Caseys C, Kliebenstein DJ. Genetic and molecular landscapes of the generalist phytopathogen Botrytis cinerea. Molecular Plant Pathology. 2024;25(1):e13404. doi:10.1111/mpp.13404

55. Soltis NE, Atwell S, Shi G, Fordyce R, Gwinner R, Gao D, Shafi A, Kliebenstein DJ. Interactions of Tomato and *Botrytis cinerea* Genetic Diversity: Parsing the Contributions of Host Differentiation, Domestication, and Pathogen Variation. The Plant Cell. 2019;31(2):502–519. doi:10.1105/tpc.18.00857

56. Spanner R, Taliadoros D, Richards J, Rivera-Varas V, Neubauer J, Natwick M, Hamilton O, Vaghefi N, Pethybridge S, Secor GA, et al. Genome-Wide Association and Selective Sweep Studies Reveal the Complex Genetic Architecture of DMI Fungicide Resistance in

Cercospora beticola. Genome Biology and Evolution. 2021;13(9):evab209. doi:10.1093/gbe/evab209

57. Tang M, Wang Y, Wang K, Zhou Y, Zhao E, Zhang H, Zhang M, Yu H, Zhao X, Li G. Codon Optimization Enables the Geneticin Resistance Gene to Be Applied Efficiently to the Genetic Manipulation of the Plant Pathogenic Fungus Botrytis cinerea. Plants. 2024;13(2):324. doi:10.3390/plants13020324

58. Taniguchi S, Hosokawa-Shinonaga Y, Tamaoki D, Yamada S, Akimitsu K, Gomi K. Jasmonate induction of the monoterpene linalool confers resistance to rice bacterial blight and its biosynthesis is regulated by JAZ protein in rice. Plant, Cell & Environment. 2014;37(2):451–461. doi:10.1111/pce.12169

59. Thomas G, Rusman Q, Morrison WR, Magalhães DM, Dowell JA, Ngumbi E, Osei-Owusu J, Kansman J, Gaffke A, Pagadala Damodaram KJ, et al. Deciphering Plant-Insect-Microorganism Signals for Sustainable Crop Production. Biomolecules. 2023;13(6):997. doi:10.3390/biom13060997

60. Van Kan JAL, Stassen JHM, Mosbach A, Van Der Lee TAJ, Faino L, Farmer AD, Papasotiriou DG, Zhou S, Seidl MF, Cottam E, et al. A gapless genome sequence of the fungus *Botrytis cinerea*. Molecular Plant Pathology. 2017;18(1):75–89. doi:10.1111/mpp.12384

61. Vela-Corcía D, Aditya Srivastava D, Dafa-Berger A, Rotem N, Barda O, Levy M. MFS transporter from Botrytis cinerea provides tolerance to glucosinolate-breakdown products and is required for pathogenicity. Nature Communications. 2019;10(1):2886. doi:10.1038/s41467-019-10860-3

62. Vivaldo G, Masi E, Taiti C, Caldarelli G, Mancuso S. The network of plants volatile organic compounds. Scientific Reports. 2017;7(1):11050. doi:10.1038/s41598-017-10975-x

63. Westrick NM, Smith DL, Kabbage M. Disarming the Host: Detoxification of Plant Defense Compounds During Fungal Necrotrophy. Frontiers in Plant Science. 2021 [accessed 2025 Dec 17];12. https://www.frontiersin.org/journals/plant-science/articles/10.3389/fpls.2021.651716/full. doi:10.3389/fpls.2021.651716

64. Wu Z, Bi Y, Zhang J, Gao T, Li X, Hao J, Li G, Liu P, Liu X. Multidrug resistance of Botrytis cinerea associated with its adaptation to plant secondary metabolites. mBio. 15(2):e02237-23. doi:10.1128/mbio.02237-23

65. Xu Y, Tong Z, Zhang X, Wang Y, Fang W, Li L, Luo Z. Unveiling the Mechanisms for the Plant Volatile Organic Compound Linalool To Control Gray Mold on Strawberry Fruits. Journal of Agricultural and Food Chemistry. 2019;67(33):9265–9276. doi:10.1021/acs.jafc.9b03103

66. You Y, Suraj HM, Matz L, Herrera Valderrama AL, Ruigrok P, Shi-Kunne X, Pieterse FPJ, Oostlander A, Beenen HG, Chavarro-Carrero EA, et al. Botrytis cinerea combines four molecular strategies to tolerate membrane-permeating plant compounds and to increase virulence. Nature Communications. 2024;15(1):6448. doi:10.1038/s41467-024-50748-5

67. Zheng W, Wuyun Q, Li Y, Liu Q, Zhou X, Peng C, Zhu Y, Freddolino L, Zhang Y. Deep-learning-based single-domain and multidomain protein structure prediction with D-I-TASSER. Nature Biotechnology. 2025 May 23:1–13. doi:10.1038/s41587-025-02654-4

68. Zhou X, Stephens M. Genome-wide efficient mixed-model analysis for association studies. Nature Genetics. 2012;44(7):821–824. doi:10.1038/ng.2310